

An Investigation of the Charge Conservation Problem for MOSFET Circuit Simulation

PING YANG, BERTON D. EPLER, AND PALLAB K. CHATTERJEE, MEMBER, IEEE

Abstract—MOSFET capacitor models implemented in circuit simulators currently do not guarantee charge conservation, which is extremely crucial for the simulation of dynamic RAM's, switched capacitor filters, and other MOS VLSI circuits. Several MOSFET capacitor models have been introduced in the literature; however, none of these models addresses the actual reasons of charge nonconservation in SPICE2. This charge conservation problem has been studied and the causes are found. Our investigations show that charge is the appropriate state variable, and that the nonconservation of charge in SPICE2 stems from a numerical integration problem quite independent of the device physics. A new charge model has been derived, implemented in SPICE2, and tested. The new model differs from the previous models in two respects. First, it uses both charge equations and capacitance equations. Second, the partitioning of the channel charge between the source and drain terminals is carried out by requiring the charge equations to satisfy self-consistent boundary conditions. A strong emphasis is placed on charge continuity, both in the conventional operating region and in the region of weak inversion and accumulation. Benchmark tests indicate that this new model conserves charge while reducing the simulation time by 18–85 percent compared to Meyer's model which was originally used in SPICE2.

I. INTRODUCTION

CHARGE conservation is extremely crucial for the simulation of some important MOS devices and circuits, such as dynamic RAM's and switched capacitor circuits. Meyer's capacitance model is used in SPICE2 [1], [2]. In recent years, attempts to resolve the charge conservation problem have been published in the literature [3], [4]. These efforts have assumed that the charge conservation may be achieved through more accurate representation of the device physics. In [3], nonreciprocal capacitances were introduced and the inclusion of source-bulk and drain-bulk capacitances were considered to be required for charge conservation. In [4], a four-terminal equivalent circuit was introduced and the author claimed that this new equivalent circuit will conserve charge. In this paper, we present the results of our investigation which show that the charge nonconservation is a problem of numerical integration and that the accuracy of the device model and the charge conservation in transient analysis are independent.

In general, either charge or voltage can be chosen as the state variable; however, this is not true for MOS capacitors. An

Manuscript received February 25, 1982; revised July 15, 1982. This work was supported in part by DARPA Contract MDA 903-78-C-0296. Part of this paper was presented at the 39th Device Research Conference, April 1981.

The authors are with Texas Instruments, Inc., Dallas, TX 79265.

example is presented in this paper to show why charge should be chosen as the state variable for MOS circuit simulation.

We show that with charge $Q(V)$ as the state variable, the accuracy of the capacitances (dQ/dV) is not important as far as the accuracy of the transient analysis is concerned because the capacitances are only used in the Newton-Raphson iterations. So the four-terminal equivalent circuits presented in [4] do not guarantee accurate transient analysis and are not the solution of the charge conservation problem in SPICE2. We must concentrate on representing the charge $Q(V)$ correctly to impact this problem.

A new charge model is presented in this paper. This new charge model is derived for accurate circuit simulation and charge conservation. The derivation takes into account the fact that the charges must be continuous throughout all different regions in order to be useful for circuit simulation programs such as SPICE2 [2].

This new charge model has been implemented in SPICE2 and has been tested thoroughly using circuits with 1–1500 devices.

II. NUMERICAL METHOD

Since the key elements of the derivation of the charge-conserving capacitor model presented in this paper are based on the numerical techniques used for the implementation of the model in SPICE2, we shall present a brief review of the techniques in this section for the benefit of the readers who are not familiar with these methods. Readers who are more familiar with these techniques are advised to skip to Section III.

A numerical integration method is required to determine the transient response of a circuit. There are many different stiffly stable numerical integration algorithms used within SPICE2; however, for simplicity of the discussion, let us assume that we use the trapezoidal method for a linear capacitor. The discretized time domain solution $v(n+1)$ is given by

$$v(n+1) = v(n) + \frac{h(n)}{2} (\dot{v}(n+1) + \dot{v}(n)) \quad (1)$$

where $h(n) = t(n+1) - t(n)$.

In the above expression, $\dot{v}(n+1)$ and $\dot{v}(n)$ have been averaged together to approximate the mean value derivative.

Substituting the branch relationship for a capacitor

$$i = C\dot{v} \quad (2)$$

into (1), we obtain

$$v(n+1) = v(n) + \frac{h(n)}{2} \left(\frac{i(n+1)}{C(n+1)} + \frac{i(n)}{C(n)} \right) \quad (3)$$

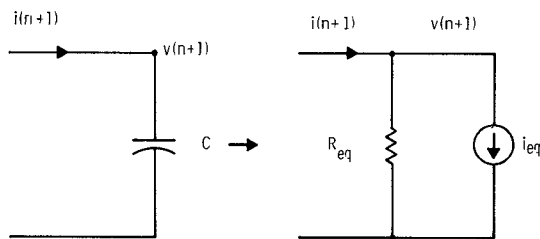


Fig. 1. Discrete companion model associated with the trapezoidal method for a capacitor.

and solving for $i(n+1)$ gives

$$\begin{aligned} i(n+1) &= -\left(\frac{C(n+1)}{C(n)}\right) i(n) + \frac{2}{h(n)} C(n+1) v(n) \\ &\quad + \frac{2C(n+1)}{h(n)} v(n+1) \\ &= i_{eq} + v(n+1)/R_{eq}. \end{aligned} \quad (4)$$

The relationship given by (4) can be represented by the equivalent companion model shown in Fig. 1.

The use of discrete companion model reduces the transient analysis of a dynamic network to the dc analysis of a resistive network.

III. CHOICE OF STATE VARIABLES

To obtain a transient circuit response, the common choice of state variables are capacitor voltages. From the computational point of view, however, it is advantageous to choose Q as the state variable [5] when the circuits contain nonlinear capacitors. The choice of Q as the state variable can be shown to result in less error propagation. For MOSFET capacitors, the situation is different. The choice of Q as the state variable becomes essential, since the nonlinear MOSFET capacitors are not controlled only by their terminal voltages alone. For example, C_{gs} is controlled by V_{gs} , V_{ds} , and V_{bs} . The choice of Q as the state variable for MOSFET capacitors makes the circuit simulator more general and more efficient. The following example illustrates the importance of choosing Q as the state variable if a nonlinear capacitor is controlled by voltages other than its terminal voltage.

Example 1: Consider a circuit consisting of a nonlinear capacitor C_1 and linear capacitor C_2 , as shown in Fig. 2(a).

In this example, the capacitor C_1 is controlled by v_3 as shown in Fig. 2(b). At $t = 0+$, v_3 changes from 0 to 5 V instantaneously, so C_1 changes from C_a to C_b . This problem may be solved analytically, and $v_2(0+)$ is given by

$$v_2(0+) = \frac{C_2 + C_a}{C_2 + C_b} v_2(0-) + \frac{C_b - C_a}{C_2 + C_b} v_1. \quad (5)$$

If this problem is solved by numerical integration, such as the trapezoidal integration formula reviewed in Section II, and the node voltages are chosen as the state variables, then for

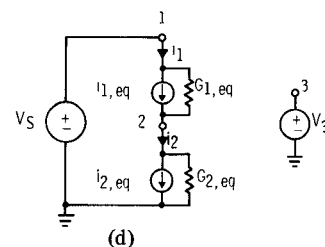
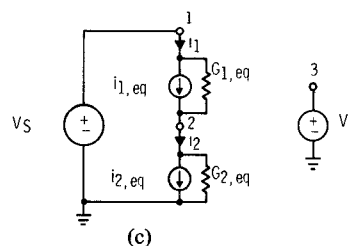
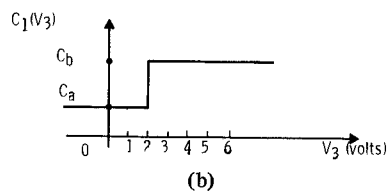
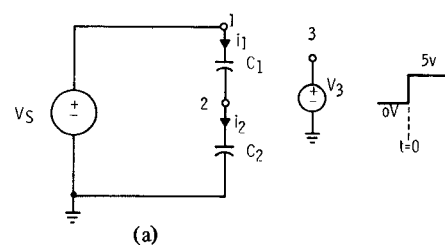


Fig. 2. (a) Example circuit. (b) C_1 as a function of v_3 . (c) Companion models for C_1 and C_2 when the node voltages are chosen as the state variables where

$$i_{1eq} = \frac{-C_1(n+1)}{C_1(n)} i(n) - \frac{2}{h(n)} C_1(n+1) v_{12}(n)$$

$$G_{1eq} = \frac{2}{h(n)} C_1(n+1)$$

$$i_{2eq} = -i(n) - \frac{2}{h(n)} - C_2 v_2(n)$$

$$G_{2eq} = \frac{2}{h(n)} C_2.$$

(d) Companion models for C_1 and C_2 when the charges are chosen as the state variables where

$$i'_{1eq} = -i(n) - \frac{2}{h(n)} C_1(n) v_{12}(n)$$

$$G'_{1eq} = \frac{2}{h(n)} C_1(n+1)$$

$$i'_{2eq} = -i(n) - \frac{2}{h(n)} C_2 v_2(n)$$

$$G'_{2eq} = \frac{2}{h(n)} C_2.$$

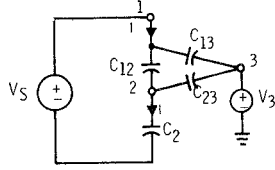


Fig. 3. Equivalent circuit including capacitances C_{13} and C_{23} for Example 1.

capacitor C_1 ,

$$i(n+1) = -\frac{C_1(n+1)}{C_1(n)} i(n) - \frac{2}{h(n)} C_1(n+1) v_{12}(n) + \frac{2}{h(n)} C_1(n+1) v_{12}(n+1). \quad (6)$$

For capacitor C_2 ,

$$i(n+1) = -\frac{2}{h(n)} C_2 v_2(n) + \frac{2}{h(n)} C_2 v_2(n+1) \quad (7)$$

where the branch relationship used for a capacitor is $i = C\dot{v}$.

The companion models [6] given by (6) and (7) are shown in Fig. 2(c).

Solving the equivalent circuit, we obtain

$$v_2(h) = v_2(0-) \quad (8)$$

where $h = h(0)$. No matter how small h is, $v_2(h)$ is stuck at $v_2(0-)$. Comparing (8) to (5), it is obvious that we have the wrong solution and that the charge is not conserved. This anomalous result, of course, can be traced back to the use of the branch relationship $i = C\dot{v}$ for the nonlinear capacitor C_1 . In reality, the description should have been

$$i = \frac{dQ}{dt} = C\dot{v} + v\dot{C}. \quad (9)$$

We can rewrite (9) for capacitor C_1 as follows. At node 1,

$$i = \frac{dQ}{dt} = \frac{\partial Q}{\partial v_{12}} \dot{v}_{12} + \frac{\partial Q}{\partial v_{13}} \dot{v}_{13} = C_{12} \dot{v}_{12} + C_{13} \dot{v}_{13}. \quad (10)$$

At node 2,

$$-i = \frac{d(-Q)}{dt} = \frac{\partial(-Q)}{\partial v_{21}} \dot{v}_{21} + \frac{\partial(-Q)}{\partial v_{23}} \dot{v}_{23} \quad (11)$$

$$i = C_{12} \dot{v}_{12} + C_{23} \dot{v}_{32}. \quad (12)$$

In the presence of time-varying capacitor C_1 , $\dot{C}v$ is not zero, that is, C_{13} and C_{23} are not zero. In order to obtain correct results, we need to include capacitances C_{13} and C_{23} in our equivalent circuit, as shown in Fig. 3.

However, since $\dot{C} = \infty$ for capacitor C_1 , C_{13} and C_{23} cannot be defined. This results in the error above.

If the charges are chosen as the state variables, then for capacitor C_1 ,

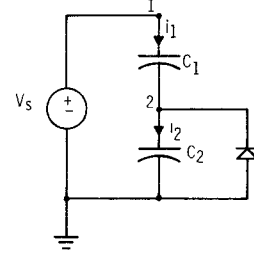


Fig. 4. Test circuit of linear capacitors and diode.

$$\begin{aligned} i(n+1) &= -i(n) - \frac{2}{h(n)} Q_1(n) + \frac{2}{h(n)} Q_1(n+1) \\ &= -i(n) - \frac{2}{h(n)} C_1(n) v_{12}(n) \\ &\quad + \frac{2}{h(n)} C_1(n+1) v_{12}(n+1). \end{aligned} \quad (13)$$

For capacitor C_2 ,

$$\begin{aligned} i(n+1) &= -i(n) - \frac{2}{h(n)} Q_2(n) + \frac{2}{h(n)} Q_2(n+1) \\ &= -i(n) - \frac{2}{h(n)} C_2 v_2(n) + \frac{2}{h(n)} C_2 v_2(n+1) \end{aligned} \quad (14)$$

where the branch relationship used for a capacitor is $Q = Cv$.

The companion models given by (13) and (14) are shown in Fig. 2(d). Solving the equivalent circuit, we obtain

$$v_2(h) = \frac{C_2 + C_a}{C_2 + C_b} v_2(0-) + \frac{C_b - C_a}{C_2 + C_b} v_1 \quad (15)$$

which gives the correct result and is the same as the analytic solution. It can now be seen from the previous example that the selection of voltage as the state variable is not the proper choice.

IV. CHARGE CONSERVATION PROBLEM

The investigation of the charge conservation problem for the MOS capacitor model has been divided into two parts. In the first part, test circuits were developed to identify all the possible reasons for this problem. In the second part, the results obtained from the first part were used to develop a new model which conserves charge. In all the tests, the time step has been chosen small enough to minimize charge loss due to discretization.

The first test circuit is shown in Fig. 4. In this circuit, both C_1 and C_2 are linear capacitors. It was found that even with linear capacitors, charge nonconservation still occurred. Investigation shows that this is due to the choice of inappropriate error tolerances. At every iteration or time point, a current tolerance δI , a voltage tolerance δV , and a charge tolerance δQ are allowed. If those tolerances are not chosen properly, the accumulated errors will show up as nonconservation of charge. The second test circuit is shown in Fig. 5. In this circuit, C_1 is a one-dimensional polynomial capacitor; the controlling argu-

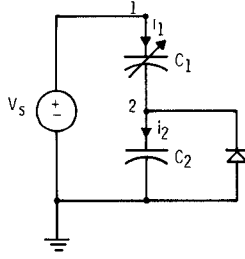


Fig. 5. Test circuit of one-dimensional polynomial capacitor.

ment is chosen to be the terminal voltage. C_2 is a linear capacitor.

Even with very tight error tolerances, we found that charge was not conserved. This problem is due to the fact that in SPICE2, only the node voltages v_1 and v_2 are checked to satisfy the following condition:

$$|v_n^{k+1} - v_n^k| \leq \epsilon_a + \epsilon_r \max(|v_n^{k+1}|, |v_n^k|) \quad n = 1, 2 \quad (16)$$

where ϵ_a and ϵ_r are absolute and relative error tolerances. The terminal voltages (i.e., $v_1 - v_2$) and charges Q_1 and Q_2 of capacitors are not checked. Although the changes of the node voltages v_1 and v_2 are within the iteration error tolerances, the changes of the terminal voltages (i.e., $v_1 - v_2$) and charges Q_1 and Q_2 of the capacitors may still be large percentage-wise. This will cause charge nonconservation. This error may be eliminated by implementing the checking of capacitor terminal voltages and charges.

We then used test circuits of MOSFET capacitors; charge nonconservation was observed even with proper error tolerances and proper convergence checks. We found that this is due to the fact that charges are the state variables used in SPICE2, but the charge equations are not available in the MOSFET model; only the capacitance equations are available, so that charges are obtained through approximation $Q = \int C(v) dv$, and thus are path dependent. However, charge conservation requires $Q(v)$ to be analytic, that is, $Q(v)$ cannot be path dependent. Thus, in order to have charge conservation results, we need to have charge equations instead of capacitance equations.

V. THE NEW CHARGE MODEL

The MOSFET device can be partitioned into intrinsic and extrinsic regions as shown in Fig. 6. The extrinsic regions can be modeled by fixed overlap and lateral diffusion capacitances plus drain and source p-n junction capacitances and sidewall capacitances. Those capacitances are either constants or are controlled only by their own terminal voltages, so the charge model can be obtained by integration of $C(v) dv$.

The modeling of the intrinsic regions is more complicated because the capacitances are controlled by voltages other than their own terminal voltages. The charge model equations must be analytic in each region and be continuous throughout different regions in order to be useful for circuit simulation.

The MOSFET capacitors are controlled by V_g , V_b , V_d , and V_s ; so we need four sets of charge equations Q_g , Q_b , Q_d , and Q_s , where $Q_d + Q_s$ is the channel mobile charge Q_c .

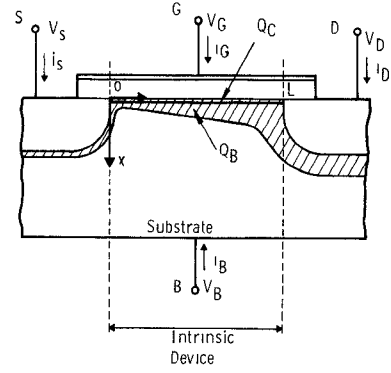


Fig. 6. MOSFET device.

The charge model equations in the linear and saturation regions are derived from the dc current model [7]. The charge model equations in the subthreshold and accumulation regions are derived from solving one-dimensional Poisson equations [8], [9]. Special attention has been paid to make sure those charges are continuous throughout different regions. In the above derivation, we assumed that the mobile charge beyond the pinchoff point are small and can be neglected. Also, charges derived above have not included the drain depletion charges.

Let the values q_g , q_c , and q_b represent the charge densities per unit area on gate, in channel, and in substrate depletion layer. The charge equations in different regions are given below.

1) *Linear Region:* $V_{gs} \geq V_{gsat}$

$$q_g = C_{ox}(V_{gs} - V_{FB} - 2\phi_f - V_y) \quad (17)$$

$$q_c = -C_{ox}(V_{gs} - V_T - \alpha_x V_y) \quad (18)$$

$$q_b = -C_{ox}(V_T - V_{FB} - 2\phi_f - (1 - \alpha_x) V_y) \quad (19)$$

where V_{gs} is the gate-to-source voltage, V_y is the quasi-Fermi potential for electrons and is defined with respect to the source, $\alpha_x = \alpha + \gamma(V_{gs} - V_T)$, α and γ are short channel parameters,

$$V_{gsat} = V_T + \alpha_x V_{ds},$$

$$V_{FB} = \phi_{MS} - \frac{Q_{SS}}{C_{ox}},$$

and

$$V_T = V_{FB} + 2\phi_f + BE \sqrt{2\phi_f - V_{bs}}.$$

After carrying out the integration,

$$\begin{aligned} Q_g &= W \int_0^L q_g dy \\ &= \text{W.L. } C_{ox} \left(V_{gs} - V_{FB} - 2\phi_f - \frac{V_{ds}}{2} \right. \\ &\quad \left. + \frac{\alpha_x V_{ds}^2}{12 \left(V_{gs} - V_T - \frac{\alpha_x V_{ds}}{2} \right)} \right) \quad (20) \end{aligned}$$

$$Q_b = \text{W.L. } C_{\text{ox}} \left(V_{FB} + 2\phi_f - V_T + \frac{(1 - \alpha_x)}{2} V_{ds} - \frac{(1 - \alpha_x) \alpha_x V_{ds}^2}{12 \left(V_{gs} - V_T - \frac{\alpha_x}{2} V_{ds} \right)} \right) \quad (21)$$

$$Q_c = -\text{W.L. } C_{\text{ox}} \left(V_{gs} - V_T - \frac{\alpha_x}{2} V_{ds} + \frac{\alpha_x^2 V_{ds}^2}{12 \left(V_{gs} - V_T - \frac{\alpha_x}{2} V_{ds} \right)} \right) \quad (22)$$

2) *Saturation Region:* $V_T \leq V_{gs} < V_{gsat}$

$$Q_g = \text{W.L. } C_{\text{ox}} \left(V_{gs} - V_{FB} - 2\phi_f - \frac{(V_{gs} - V_T)}{3\alpha_x} \right) \quad (23)$$

$$Q_b = \text{W.L. } C_{\text{ox}} \left(V_{FB} + 2\phi_f - V_T + \frac{(1 - \alpha_x)(V_{gs} - V_T)}{3\alpha_x} \right) \quad (24)$$

$$Q_c = -\text{W.L. } C_{\text{ox}} \left(\frac{2}{3} (V_{gs} - V_T) \right) \quad (25)$$

3) *Subthreshold Region:* $V_{FB} + V_{bs} \leq V_{gs} < V_T$

$$Q_g = \text{W.L. } C_{\text{ox}} \cdot \frac{BE^2}{2} \left(-1 + \sqrt{1 + \frac{4(V_{gs} - V_{FB} - V_{bs})}{BE^2}} \right) \quad (26)$$

$$Q_b = -Q_g \quad (27)$$

$$Q_c = 0. \quad (28)$$

4) *Accumulation Region:*

$$Q_g = \text{W.L. } C_{\text{ox}} (V_{gs} - V_{FB} - V_{bs}) \quad (29)$$

$$Q_b = -Q_g \quad (30)$$

$$Q_c = 0. \quad (31)$$

The charge Q_c is partitioned into Q_d and Q_s by considering the following self-consistent boundary conditions.

1) In the saturation region, the channel is isolated from the drain, so all the channel mobile charge Q_c goes into Q_s and Q_d is zero.

2) Charges Q_d and Q_s are continuous from the saturation region throughout the linear region.

3) The capacitances C_{dg} and C_{sg} are equal and the charges Q_d and Q_s are equal when V_{ds} is zero.

4) The capacitances C_{dg} , C_{ds} , C_{db} , C_{sg} , C_{sd} , and C_{sb} are continuous from the saturation region throughout the linear region.

According to the above boundary conditions, Q_d and Q_s are given as follows.

1) *Saturation Region:*

$$Q_d = 0 \quad (32)$$

$$Q_s = -\text{W.L. } C_{\text{ox}} \left(\frac{2}{3} (V_{gs} - V_T) \right) \quad (33)$$

2) *Linear Region:*

$$Q_d = -\text{W.L. } C_{\text{ox}} \left(\frac{(V_{gs} - V_T)}{2} - \frac{3}{4} \alpha_x V_{ds} + \frac{\alpha_x^2 V_{ds}^2}{8 \left(V_{gs} - V_T - \frac{\alpha_x}{2} V_{ds} \right)} \right) \quad (34)$$

$$Q_s = -\text{W.L. } C_{\text{ox}} \left(\frac{(V_{gs} - V_T)}{2} + \frac{\alpha_x V_{ds}}{4} - \frac{\alpha_x^2 V_{ds}^2}{24 \left(V_{gs} - V_T - \frac{\alpha_x}{2} V_{ds} \right)} \right) \quad (35)$$

The reasoning for condition 1) partitioning is given below. In order to derive the charges Q_g , Q_b , and Q_c as functions of the terminal voltages, the steady-state current continuity and Poisson equations were used instead of the transient transport equations, that is, the instantaneous variations of those charges to reach the steady-state values are not modeled. Therefore, the charges Q_d and Q_s are the charges electrostatically associated with the drain and the source. In the saturation region, the charges electrostatically associated with the drain are the mobile charges beyond the pinchoff point and the drain depletion charges. Since these two charges are neglected in the calculation of Q_c , then the partitioning of all the channel charge Q_c into Q_s in the saturation region is a reasonable assumption.

VI. IMPLEMENTATION OF THE CHARGE MODEL IN CIRCUIT SIMULATION PROGRAM

The currents and charges are related by

$$i_g = \frac{dQ_g}{dt} \quad (36)$$

$$i_b = \frac{dQ_b}{dt} \quad (37)$$

$$i_d = \frac{dQ_d}{dt} \quad (38)$$

$$i_s = \frac{dQ_s}{dt} \quad (39)$$

Let subscripts denote nodes and superscripts denote Newton-Raphson iteration numbers. The numerical integration algorithm used is the trapezoidal method or any of Gear's stiffly stable algorithms. For example, if we use the trapezoidal method, then we can write

$$Q_l(n+1) = Q_l(n) + \frac{h(n)}{2} (\dot{Q}_l(n+1) + \dot{Q}_l(n)) = g, b, d, s. \quad (40)$$

Substituting $i_l = dQ_l/dt$ into (40), we obtain the companion models at nodes g , d , b , and s :

$$i_l(n+1) = -i_l(n) + \frac{2}{h(n)} (Q_l(n+1) - Q_l(n)) \quad l = g, b, d, s. \quad (41)$$

Then the Newton-Raphson method can be used to linearize the companion models and obtain the solutions, that is,

$$\begin{aligned} i_l^{k+1}(n+1) &= i_l^k(n+1) \\ &+ \sum_{m \neq l} \frac{\partial i_l}{\partial V_{lm}^k} (V_{lm}^{k+1}(n+1) - V_{lm}^k(n+1)) \\ &= -i_l(n) + \frac{2}{h(n)} (Q_l^k(n+1) - Q_l(n)) \\ &+ \sum_{m \neq l} \frac{2}{h(n)} \frac{\partial Q_l}{\partial V_{lm}^k} (V_{lm}^{k+1}(n+1) - V_{lm}^k(n+1)) \end{aligned} \quad l = g, b, d, s. \quad (42)$$

Let us define

$$C_{lm}^k = \frac{\partial Q_l}{\partial V_{lm}^k} \quad l \neq m, \quad l = g, b, d, s. \quad (43)$$

Then (42) can be written as

$$\begin{aligned} i_l^{k+1}(n+1) &= i_l(n) + \frac{2}{h(n)} (Q_l^k(n+1) - Q_l(n)) \\ &+ \sum_{m \neq l} \frac{2}{h(n)} (C_{lm}^k (V_{lm}^{k+1}(n+1) - V_{lm}^k(n+1))) \\ &= i_{l,eq}^k + \sum_{m \neq l} \frac{2}{h(n)} C_{lm}^k V_{lm}^{k+1}(n+1) \end{aligned} \quad l = g, b, d, s \quad (44)$$

where

$$\begin{aligned} i_{l,eq}^k &= i_l(n) + \frac{2}{h(n)} (Q_l^k(n+1) - Q_l(n)) \\ &- \sum_{m \neq l} \frac{2}{h(n)} C_{lm}^k V_{lm}^k(n+1). \end{aligned} \quad (45)$$

So the element stamp for Q_l used in the modified nodal approach [10], [11] is

$$\begin{aligned} & \begin{matrix} l & r & p & q \\ l \left[\frac{2}{h(n)} (C_{lr}^k + C_{lp}^k + C_{lq}^k) - \frac{2}{h(n)} C_{lr}^k - \frac{2}{h(n)} C_{lp}^k - \frac{2}{h(n)} C_{lq}^k \right] \\ \text{RHS} \\ [-i_{l,eq}^k]. \end{matrix} \end{aligned} \quad (46)$$

From (41) and (44), we can see that the capacitances are only used in the Newton-Raphson iterations, and thus the physical accuracy of the capacitances are not important as far as the numerical accuracy of the transient analysis is concerned. However, the charges are used to determine the transient response, so the physical accuracy of the charge models is extremely important.

In total, we need to evaluate 12 capacitances and four equivalent currents; however, there are only nine independent capacitances and three independent equivalent currents due to conservation of charge.

From conservation of charge, we have

$$Q_g + Q_b + Q_d + Q_s = 0 \quad (47)$$

$$i_g + i_b + i_d + i_s = 0. \quad (48)$$

Equations (36)-(39) can be rewritten as

$$i_g = \frac{dQ_g}{dt} = \frac{\partial Q_g}{\partial V_{gb}} \frac{dV_{gb}}{dt} + \frac{\partial Q_g}{\partial V_{gd}} \frac{dV_{gd}}{dt} + \frac{\partial Q_g}{\partial V_{gs}} \frac{dV_{gs}}{dt} \quad (49)$$

$$i_b = \frac{dQ_b}{dt} = \frac{\partial Q_b}{\partial V_{bg}} \frac{dV_{bg}}{dt} + \frac{\partial Q_b}{\partial V_{bd}} \frac{dV_{bd}}{dt} + \frac{\partial Q_b}{\partial V_{bs}} \frac{dV_{bs}}{dt} \quad (50)$$

$$i_d = \frac{dQ_d}{dt} = \frac{\partial Q_d}{\partial V_{dg}} \frac{dV_{dg}}{dt} + \frac{\partial Q_d}{\partial V_{db}} \frac{dV_{db}}{dt} + \frac{\partial Q_d}{\partial V_{ds}} \frac{dV_{ds}}{dt} \quad (51)$$

$$i_s = \frac{dQ_s}{dt} = \frac{\partial Q_s}{\partial V_{sg}} \frac{dV_{sg}}{dt} + \frac{\partial Q_s}{\partial V_{sb}} \frac{dV_{sb}}{dt} + \frac{\partial Q_s}{\partial V_{sd}} \frac{dV_{sd}}{dt}. \quad (52)$$

Substituting (49)-(52) into (48), we obtain

$$\sum_{m \neq l} C_{lm} = \sum_{m \neq l} C_{ml} \quad l = g, b, d, s. \quad (53)$$

So there are only nine independent capacitances; for example, if we choose to evaluate C_{gb} , C_{gd} , C_{gs} , C_{bg} , C_{bd} , C_{bs} , C_{dg} , C_{db} , and C_{ds} , then C_{sg} , C_{sb} , and C_{sd} can be evaluated by

$$C_{sg} = C_{gb} + C_{gd} + C_{gs} - C_{bg} - C_{dg} \quad (54)$$

$$C_{sb} = C_{bg} + C_{bd} + C_{bs} - C_{gb} - C_{db} \quad (55)$$

$$C_{sd} = C_{dg} + C_{db} + C_{ds} - C_{gd} - C_{bd}. \quad (56)$$

For the equivalent currents, summing up (44) over l and then using (48), we obtain

$$\begin{aligned} \sum_l i_l^{k+1}(n+1) &= \sum_l i_{l,eq}^k + \sum_l \sum_{m \neq l} \frac{2}{h(n)} C_{lm}^k V_{lm}^{k+1}(n+1) \\ &= 0, \end{aligned} \quad (57)$$

and from (53), we obtain

$$\sum_l \sum_{m \neq l} \frac{2}{h(n)} C_{lm}^k V_{lm}^{k+1}(n+1) = 0. \quad (58)$$

Substituting (58) into (57), we obtain

$$\sum_l i_{l,eq}^k = 0. \quad (59)$$

So if we choose to evaluate $i_{g,eq}^k$, $i_{b,eq}^k$, and $i_{d,eq}^k$, then $i_{s,eq}^k$ can be evaluated by

$$i_{s,eq}^k = -i_{g,eq}^k - i_{b,eq}^k - i_{d,eq}^k. \quad (60)$$

VII. EXAMPLES AND RESULTS

The new charge model has been implemented in TI SPICE2 and has been tested out extensively against static and dynamic

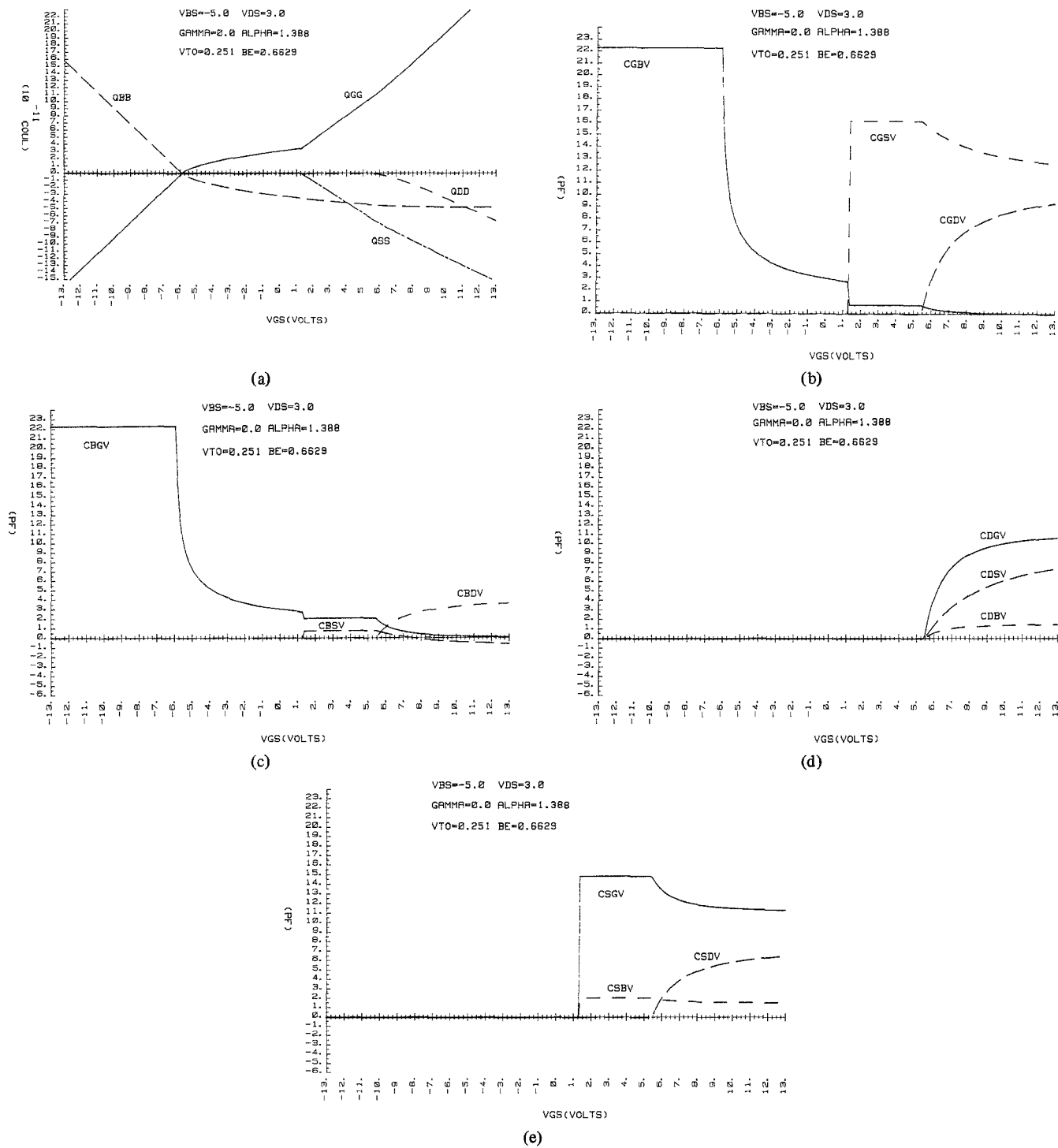


Fig. 7. (a) Charges associated with gate, bulk, drain, and source. (b) Capacitances associated with gate. (c) Capacitances associated with bulk. (d) Capacitances associated with drain. (e) Capacitances associated with source.

MOSFET circuits including SRAM's, DRAM's, switched capacitor filters, and other MOS VLSI circuits. The plots of the four charges and 12 capacitances of this new model are given in Fig. 7. Fig. 8(a) shows a simple charge pumping circuit which illustrates the usefulness of this new model. This charge pumping circuit presents a severe test for charge conservation. In this circuit, three voltages, V_{gs} , V_{ds} , and V_{bs} , are varying, and they switch at different time points [Fig. 8(b)], so the MOSFET goes through different regions by different paths. If the state

variable, charge, is path dependent, then charge nonconservation will be observed. The simulated output using Meyer's model is shown in Fig. 8(c). Due to charge nonconservation, the output voltage changes from one cycle to the other cycle no matter how small the tolerances and time steps are. Fig. 8(d) shows the simulated output using the new model. With appropriate tolerances and time steps, the output voltage remains at the correct level from one cycle to the other cycle. This shows that the new model conserves charge. Also, Fig.

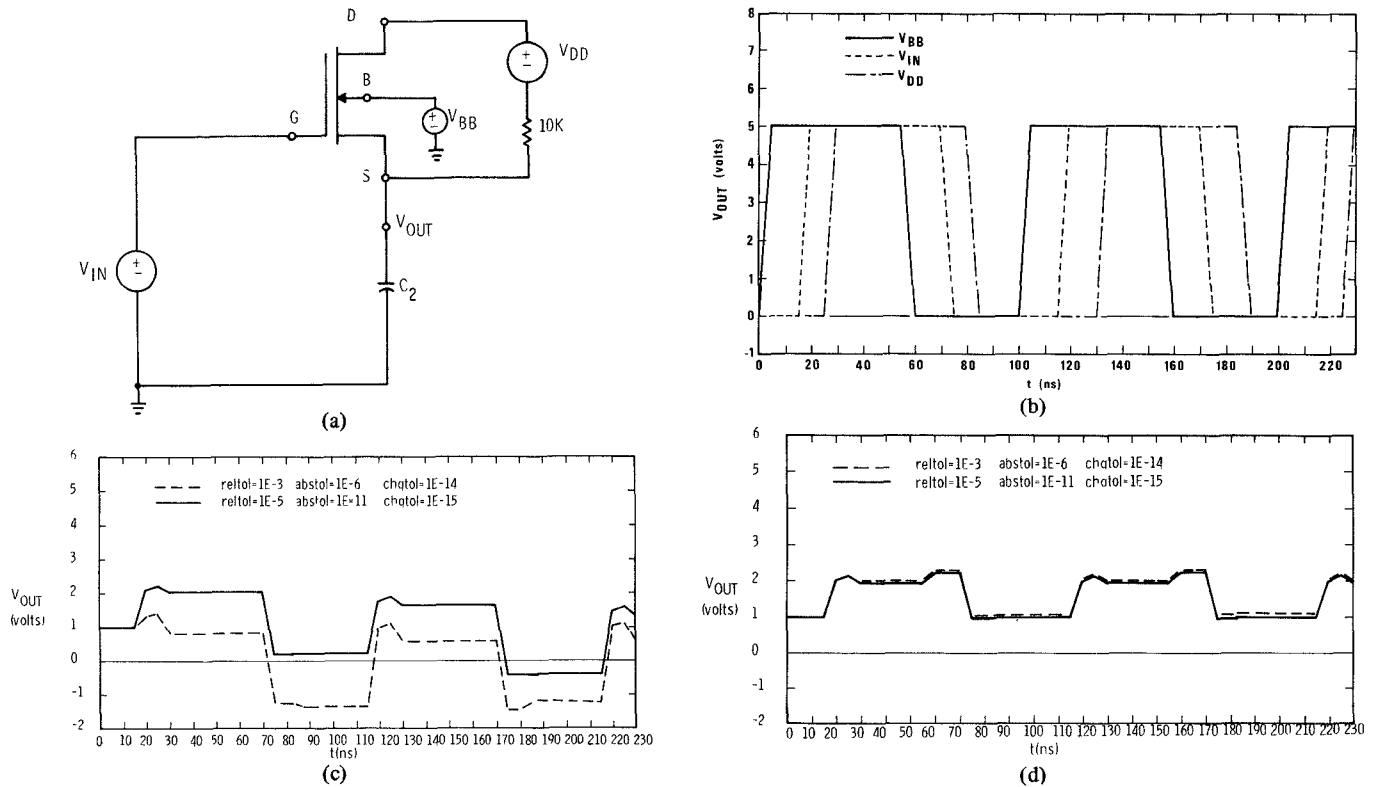


Fig. 8. (a) Test circuit of a MOSFET capacitor and a linear capacitor. (b) Waveforms of input signals V_{in} , V_{BB} , and V_{DD} . (c) Simulated output using Meyer's model. (d) Simulated output using the new charge model.

8(d) shows that with loose tolerances, the output voltage still has small changes from one cycle to the other cycle, which is consistent with our investigation results presented in Section IV. However, these small changes of the output voltage are much smaller than the changes of the output voltage with Meyer's model and tight tolerances. That is, with this new charge model, the simulation time can be reduced while maintaining better accuracy. Fig. 9(a) is the circuit of a switched capacitor low-pass filter. The two clocks ϕ_A and ϕ_B are given in Fig. 9(b). The simulated output using Meyer's model is shown in Fig. 9(c). According to Meyer's model, the output V_6 has reached steady state. However, the waveform of V_3 indicates that there is a large charge transfer between nodes 1 and 3, that is, V_6 cannot be in steady state. The results are conflicting and nonphysical, and the cause is charge nonconservation. Fig. 9(d) shows the simulated output using the new charge model. The waveforms of V_3 and V_6 are consistent, and the charge transfers in phases ϕ_A and ϕ_B are equal. Moreover, V_6 rises with the correct time constant as predicted by switched capacitor theory.

Also, with this new charge model, we have an explicit expression for the charge, so the estimates of the truncation errors can be made more accurate [12]. This helps to reduce simulation time ever further.

Several static and dynamic MOSFET circuits were analyzed with this new charge model. The size of the circuits ranges from 1 to 1515 transistors. In addition to the increased accuracy, the circuit simulation time is reduced by 18–85 percent compared to Meyer's model. Part of the results are given in Table I.

TABLE I
SPICE2 MEYER'S MODEL/CHARGE MODEL COMPARISON

CIRCUIT	1	2	3	4	5	6
CPU Time for Transient Analysis in Seconds	12.0 (8.5)	47.4 (6.7)	74.7 (60.7)	659.4 (405.0)	56.0 (40.2)	638.1 (357.1)
Percent Reduction	29	85	18	38	28	44
Number of MOSFETS	6	1	13	145	6	250

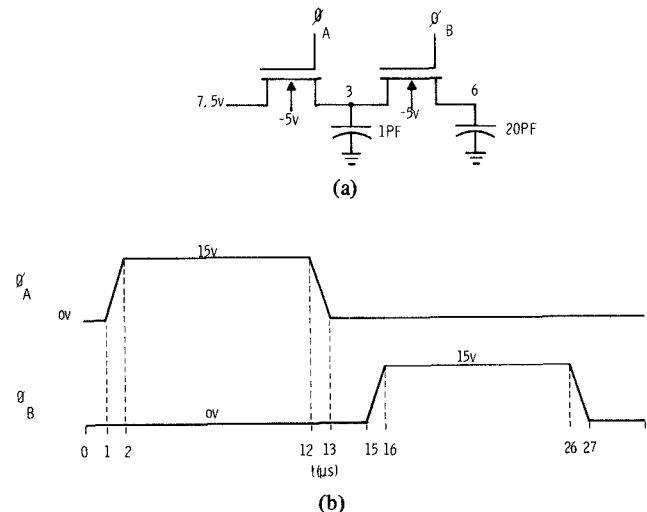


Fig. 9. (a) A switched capacitor low-pass filter circuit. (b) Waveforms of clocks ϕ_A and ϕ_B .

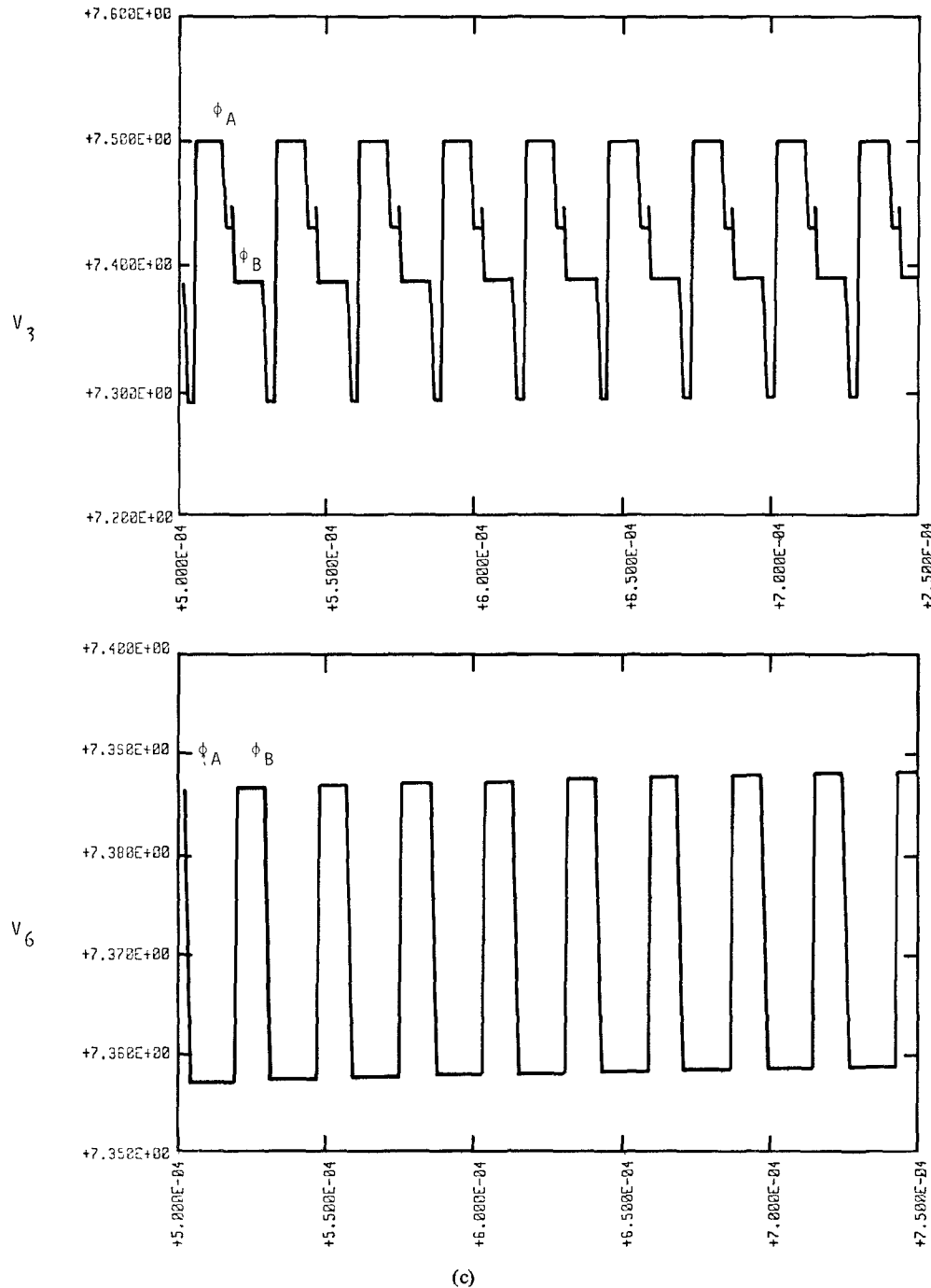


Fig. 9. (Continued.) (c) Simulated output using Meyer's mode.

VIII. CONCLUSIONS

The causes of charge nonconservation in MOS transient analysis have been found. The solutions to resolve this problem have been developed, implemented, and tested. The results indicate that a charge model is required and that the charge nonconservation in SPICE2 stems from a numerical integration problem quite independent of the device physics. If the charge is chosen as the state variable in the circuit simulator, then the physical accuracy of the capacitances are not important as far as the numerical accuracy of the transient analysis

is concerned because the capacitances are used only for the Newton-Raphson iterations. A new charge model is derived, implemented, and tested. The partitioning of the channel charge between the source and the drain is carried out by requiring the charges to satisfy self-consistent boundary conditions. The derivation emphasizes charge continuity throughout all different regions in order to be useful for circuit simulation. The model has been tested against several VLSI MOSFET circuits. The results indicate that the new model is more accurate and faster.

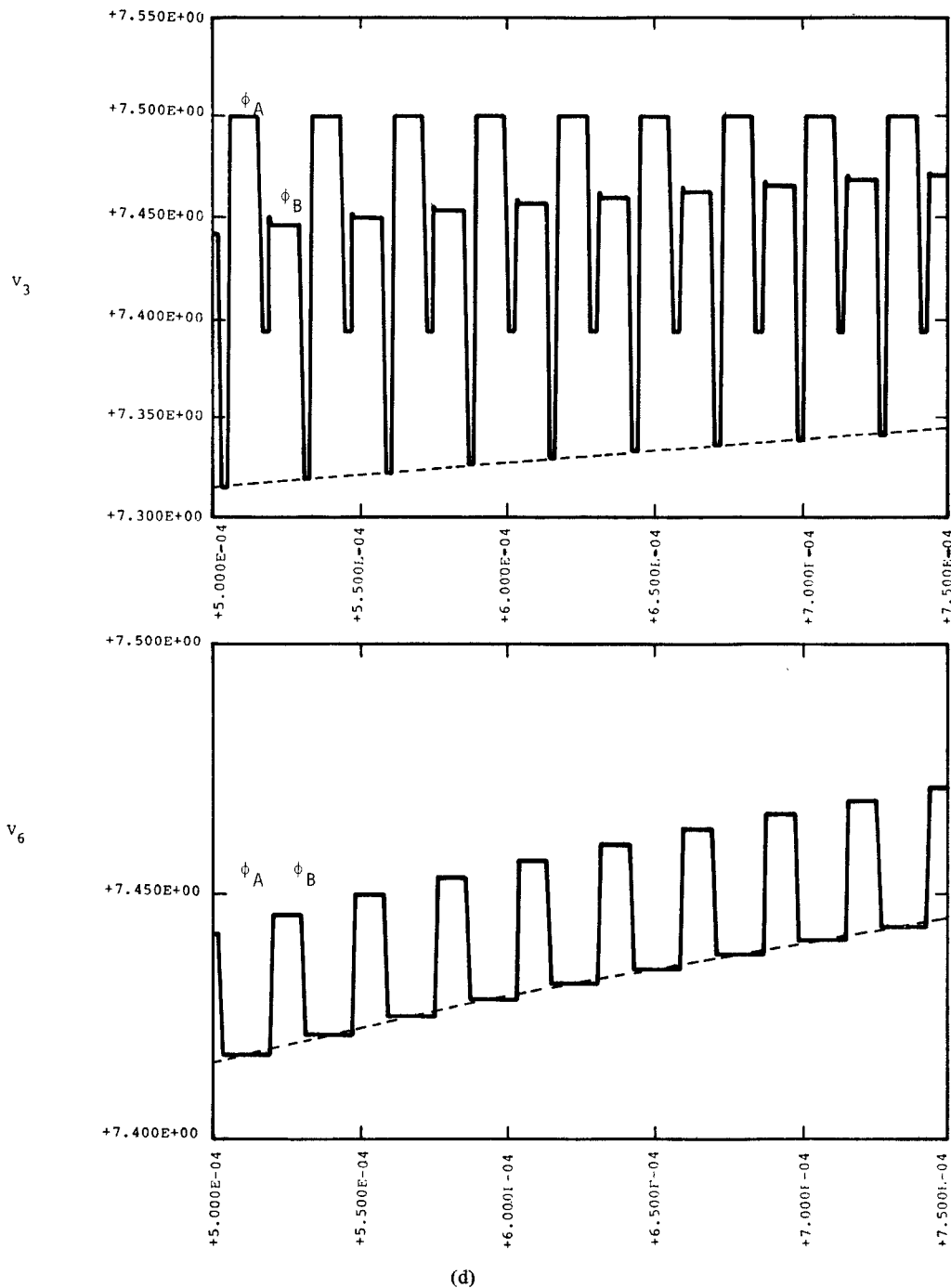


Fig. 9. (Continued.) (d) Simulated output using the new charge model.

ACKNOWLEDGMENT

The authors would like to acknowledge the helpful discussions and contributions of J. Leiss, D. Redwine, R. Colon, and D. Hester in the development of this work.

REFERENCES

[1] J. E. Meyers, "MOS models and circuit simulation," *RCA Rev.*, vol. 32, Mar. 1971.

[2] L. W. Nagel, "SPICE2: A computer program to simulate semiconductor circuits," Electron. Res. Lab., Univ. California, Berkeley, ERL Memo ERL-M520, May 1975.

[3] D. E. Ward and R. W. Dutton, "A charge-oriented model for MOS transient capacitances," *IEEE J. Solid-State Circuits*, vol. SC-13, Oct. 1978.

[4] Y. A. El-Mansy and A. R. Boothroyd, "A general four-terminal charging-current model for the insulated-gate field-effect transistor-1," *Solid State Electron.*, vol. 23, pp. 405-410, 1980.

[5] D. A. Calahan, *Computer-Aided Network Design*. New York: McGraw-Hill, 1972.

[6] L. O. Chua and P. M. Lin, *Computer-Aided Analysis of Electronic Circuits: Algorithms and Computational Techniques*. Englewood Cliffs, NJ: Prentice-Hall, 1975.

[7] *T. I. SPICE2 Users Guide*, Texas Instruments, Inc., Dallas, TX.

[8] S. M. Sze, *Physics of Semiconductor Devices*. New York: Wiley, 1969.

- [9] H. K. Ihantola and J. M. Moll, "Design theory of a surface field effect transistor," *Solid State Electron.*, vol. 7, pp. 423-430.
- [10] W. J. McCalla and D. O. Pederson, "Elements of computer-aided circuit analysis," *IEEE Trans. Circuit Theory*, vol. CT-18, pp. 14-26, Jan. 1971.
- [11] C. W. Ho, A. E. Ruehli, and P. A. Brennan, "The modified nodal approach to network analysis," *IEEE Trans. Circuits Syst.*, vol. CAS-22, pp. 504-509, June 1975.
- [12] P. Yang, "An investigation of ordering, tearing and latency algorithms for the time-domain simulation of large circuits," Univ. Illinois, Urbana-Champaign, Ph.D. dissertation, Aug. 1980.



Ping Yang was born in Ping-Tung, Taiwan, on July 15, 1952. He received the B.S. degree in physics in 1974 from National Taiwan University, Taipei, Taiwan, and the M.S. and Ph.D. degrees in electrical engineering from the University of Illinois, Urbana, in 1978 and 1980, respectively.

From 1974 to 1976 he was an Ensign in the Chinese Navy. From August 1976 to August 1980 he held a Teaching Assistantship in the Department of Electrical Engineering and a

Research Assistantship with the Coordinated Science Laboratory, University of Illinois. He joined the Central Research Laboratory, Texas Instruments, Inc., Dallas, in August 1980. His research interests are in the areas of computer-aided design, circuits and systems, large-scale integrated circuits, and solid-state electronics.

Dr. Yang is a member of Phi Kappa Phi.



Berton D. Epler was born in Arkansas City, KS, on October 31, 1937. He received the B.S.E.E. degree from Oklahoma State University, Stillwater, in 1960, and the M.S.E.E. degree from Southern Methodist University, Dallas, TX, in 1967.

He joined LTV, Garland, TX, in 1960, where he was awarded the Outstanding Young Engineer honor. He joined Collins Radio Company, Dallas, in 1964, and was responsible for support of all circuit analysis programs. He holds two patents associated with the phase sequence detector and proportional timer. He joined Texas Instruments, Inc., Dallas, in 1972, and is currently engaged as a circuit analysis consultant in the Design Automation Department.

Mr. Epler is a member of Eta Kappa Nu.



Pallab K. Chatterjee (S'74-M'76) received the B.Tech. degree in electronics and communication engineering from the Indian Institute of Technology, Kharagpur, in 1972, and the M.S.E.E. and Ph.D. degrees from the University of Illinois, Urbana-Champaign, in 1974 and 1976, respectively.

His graduate studies involved ion implantation in GaAs, GaAsP, and ZnSe to develop and characterize implanted layers for use in spontaneous and stimulated semiconductor lamps and photodetectors. He joined Texas Instruments, Inc., Dallas, TX, in 1976, where he worked on CCD memories and storage cells for dRAM's. He was involved in the development of the 64K CCD memory. Later, he worked on the modeling and fabrication of submicron MOS devices and device scaling with emphasis on the design of new structures and understanding device physics. He is currently a Texas Instruments Fellow and Manager of the VLSI Memory Design Branch of the VLSI Laboratory, Texas Instruments. His responsibilities include circuit design using innovative devices and technology and device and circuit modeling.

Dr. Chatterjee has published more than 70 articles in international scientific and technical journals and conferences, and has been awarded eight U.S. Patents. He is a member of the American Physical Society. He was awarded the President of India Gold Medal for curricular excellence and B.C.Roy Memorial Gold medal for extracurricular excellence at the Indian Institute of Technology in 1972.